Hindawi
Shock and Vibration
Volume 2024, Article ID 9043790, 23 pages
https://doi.org/10.1155/2024/9043790

Research Article

Vibration Properties of Submerged Sandwich Cylindrical Shell Based on Wave Propagation Approach: Analytical and Experimental Investigation

Guoqiang Guo,[1,2] **Yinglong Zhao**,[1,2] **and Anbin Yu**[3]

[1]*Institute of Noise and Vibration, Naval University of Engineering, Wuhan, Hubei 430033, China*
[2]*National Key Laboratory on Ship Vibration and Noise, Naval University of Engineering, Wuhan, Hubei 430033, China*
[3]*College of Power Engineering, Naval University of Engineering, Wuhan, Hubei 430033, China*

Correspondence should be addressed to Yinglong Zhao; yinglongzhao2020@163.com

Received 9 November 2023; Revised 27 February 2024; Accepted 2 April 2024; Published 24 April 2024

Academic Editor: Fabio Botta

The vibration properties of the submerged sandwich cylindrical shell with a viscoelastic core are investigated in this paper. Considering the acoustic-structure coupling, the analytical model of the submerged sandwich cylindrical shell that can handle three medium conditions including fluid-filled, fluid-loaded, and fluid-filled and -loaded is derived based on the wave propagation approach and the Flügge thin-shell theory. The vibration properties of the sandwich cylindrical shell under different medium and boundary conditions are analyzed, followed by a comparison of the damping effect of the constrained damping layer. Finally, an analysis is conducted on the influence of thicknesses of viscoelastic and constrained layers on vibration spectrum and natural frequency under fluid-filled and -loaded conditions. An experimental platform was established to conduct relevant experiments. Several important conclusions can be drawn.

1. Introduction

Constrained layer damping (CLD), which consists of a viscoelastic damping layer and a metal-constrained layer, provides an effective way to suppress undesirable mechanical vibration and wave propagation in different types of structures, such as beams [1, 2], plates [3, 4], and shells [5–7]. The fundamental principle is that the vibrational energy is dissipated during transmission through the viscoelastic damping material. The cylindrical shells are prevalent in underwater vehicles, the vibration of which can be effectively controlled by designing CLD with appropriate parameters [8]. The cylindrical shell, in which the vibration is controlled by a CLD, is referred to as a sandwich cylindrical shell. The research primarily encompasses two aspects: (1) the force-displacement relationship between the adjacent layers of the sandwich cylindrical shell and (2) the acoustic-structure coupling between the shell and the medium.

A clear comprehension of the impact of a CLD on the vibration characteristics of cylindrical shells is of utmost significance, which has attracted the attention of a growing number of scholars. Ramesh and Ganesan [9] used the finite element method (FEM) to study the vibration and damping characteristics of a sandwich cylindrical shell constrained by an isotropic surface layer. Wang and Chen [10] employed the FEM based on the discrete layer theory to derive the equations of motion of the composite system and analyze the sandwich cylindrical shell. Masti and Sainsbury [11] explored the use of a standoff-layered viscoelastic damping treatment for cylindrical shells requiring a minimal distribution area and low added weight. Abdoun et al. [12] adopted the FEM to study the forced-vibration response to curved viscoelastic shells and laminated viscoelastic shells in the frequency domain. Mohammadi and Sedaghati [13] established the linear and nonlinear models based on the FEM to study the damping characteristics of thin-core and thick-core sandwich cylindrical shells and the influences of

incomplete binding between layers, and concluded that the nonlinear model showed stronger damping characteristics than the linear model, and the slip reduces the loss factor in most modes.

Chen and Huang [14] studied the vibration response of a sandwich cylindrical shell based on the assumed-mode method and derived discrete equations of motion. Hu and Huang [15] studied the frequency response and damping effects of the sandwich cylindrical shells based on the Donnell–Mushtari–Vlasov theory, and concluded that increasing the thickness of the viscoelastic damping layer can reduce the natural frequency and damping of the system. Cao et al. [7] presented free vibration characteristics of sandwich cylindrical shells. On the basis of Sanders' thin-shell theory, the governing equations for an orthogonal anisotropic sandwich cylindrical shell were derived from the wave propagation approach, and the vibration responses of a sandwich cylindrical shell were solved under simply supported boundary conditions. Xiang et al. [16] derived governing equations describing the vibration of a sandwich cylindrical shell with a viscoelastic damping layer under harmonic excitation based on the linear theories of thin cylindrical shells and viscoelastic materials and studied the vibration characteristics and damping effect of the sandwich cylindrical shell. Based on Donnell's hypothesis, linear viscoelastic theory, and Hamiltonian principle, Zheng et al. [17] introduced state vectors to deduce the dynamic equations of a sandwich cylindrical shell in the state space, and then studied the vibration of a sandwich cylindrical shell with multiple viscoelastic damping layers. Yang et al. [18] derived the governing equations of a sandwich cylindrical shell based on first-order shear deformation theory and studied the influences of the layered scheme and structural geometric characteristics on the natural frequency and loss factor. Molhtari et al. [19] studied the vibration of sandwich cylindrical shells using the Lagrange equation and Relilitz's method, and discussed the influences of the parameters of the constrained layer on the frequency and loss factor. Shahali et al. [20] derived and solved Lagrange's equations of motion via the Rayleigh–Ritz method and studied the natural frequency and damping behavior of three-layer cylindrical shells with a viscoelastic core layer and functionally graded face layers, considering the effects of some geometrical and material parameters such as length-to-radius ratio, functionally graded properties, radius and thickness of viscoelastic layer on the natural frequency, and loss factor of the system. Mokhtari et al. [19] and Permoon et al. [21] studied the frequency and damping of sandwich cylindrical and conical shells, respectively, containing a fractional viscoelastic core and isotropic face layers. Askarian et al. [22] studied the vibration of pipes conveying fluid on a fractional viscoelastic foundation with general boundary conditions, Shitikova and Ajarmah [23] focused on the nonlinear vibrations of fractionally damped cylinders under the additive combinational internal resonance, and Permoon et al. [6] studied the nonlinear vibration of fractional cylindrical shells. All the studies mentioned above were performed in the air medium.

In the acoustic-structure coupling system underwater, due to the existence of the surrounding medium, the superposition of dry modes cannot meet the requirements. Therefore, the influences of the acoustic medium on the vibration of the structure must be introduced. At present, the research on acoustic vibration of cylindrical shells in infinite domains is extremely abundant, and major solving methods such as the wave propagation method [24], mode superposition method [25], transfer matrix method, energy method [26], and finite element coupled boundary element method [27] have been formed. Wave propagation methods expand the displacement into the form of a propagating wave and solve it directly by substituting it into the governing equation. The computational procedure is simple and the computational accuracy is elevated. The basic method chosen in this paper is the wave propagation method. Junger and Feit [25] were the first to systematically elaborate the interaction between acoustic and structure, and analyzed in detail the acoustic radiation and acoustic scattering of plates and shells based on the classical methods such as the modal superposition method and Green function method. Fuller and Fathy [28] established the dispersion equations of liquid-filled cylindrical shells. The dispersion properties of a liquid-filled cylindrical shell and the energy carried by each propagating wave were thoroughly investigated based on an iterative technique in the complex plane. Then, Fuller [29] studied the input admittance of a liquid-filled cylindrical shell under circumferential linear exciting force based on the Fourier method, and further gave the admittance expression under concentrated exciting force. Scott [30] used the Love shell theory and the energy method to derive the dispersion equations of the infinite-length underwater cylindrical shell, and solved the dispersion equations based on the complex plane iterative technique. Zhang et al. [24, 31, 32] studied the natural vibration of the acoustic-structure coupling system under various boundary conditions based on the wave propagation approach, and compared results with the FEM to verify the accuracy of the method. Guo [33] proposed an approximate method to analyze the acoustic problem of underwater cylindrical shells based on Donnell's shell theory. The acoustic radiation properties are approximately solved by the asymptotic expansion of the Hankel function. The comparison with the exact solution shows that the approximation method is accurate and reliable. Lam and Loy [26] studied the natural vibration characteristics of laminated cylindrical shells based on the Love shell theory and the energy method. The energy functional equation is obtained by introducing a beam function to fit the displacement axial function of the structure, and then the natural frequency is obtained using the Lebesgue method. Williams [34] used infinite series solutions to study the acoustic radiation characteristics of cylindrical shells. First, the velocity potential function and the boundary conditions of the cylindrical shell are expanded in terms of a series of different characteristic functions. The relation between the two types of eigenfunctions is then obtained in terms of the velocity continuity condition at the fluid-structure coupled interface. Finally, the governing equation can be solved by a finite truncation of the infinite series. Laulagnet and Guyader [27]

used the rigid sound barrier model to study the acoustic radiation characteristics of finite-length cylindrical shells in light and heavy fluids. The shell-fluid coupled governing equations were obtained by combining Fourier transform and Green's function methods, and the effect of the relative ratios of radiative loss factor and structural damping factor on the modes was discussed.

In addition, there are two aspects of the analytical method that have to be considered, which may affect the accuracy of the analytical results. First, viscoelastic damping belongs to polymer materials, and the dynamic properties of damping materials are affected by various environments such as temperature and frequency in practical engineering applications. Bagley et al. [35–39] carried out some research on viscoelastic materials. However, these factors are neglected in both analytical and numerical methods, so the AMs of sandwich structures containing viscoelastic materials have to be evaluated experimentally. Second, the simply supported boundary condition of analytical methods is not ideal for conventional boundaries in engineering applications. Qu et al. [40] improved the domain decomposition method by introducing Chebyshev orthogonal polynomials as admission functions to solve the vibration characteristics of sandwich cylindrical shells. Through a series of standard Fourier series functions, Jin et al. [41] studied the vibration characteristics of composite cylindrical shells under elastic boundaries. In the experimental construction of this paper, a simply supported boundary was approximated by an elastic boundary.

In the present study, theoretical development is first carried out considering the acoustic-structure coupling between the shell and the medium. An analytical method is presented to investigate the vibration characteristics of a sandwich cylindrical shell underwater based on the wave propagation approach. The configuration under investigation is a simple-supported sandwich cylindrical shell underwater. The studies are then conducted to investigate the coupling characteristics of the configuration under three medium conditions, including fluid-filled, fluid-loaded, and fluid-filled and -loaded, providing some research results related to vibration. The comparative experiments are carried out. Some parts of the present study have been published in the previous preprint [42].

2. Description of Sandwich Cylindrical Shells

2.1. Analytical Model. Before establishing the analytical model, the following two prerequisites should be proposed. (a) The displacements of three layers satisfy the continuity, and the radial displacements of the three layers are assumed to be equal. The resulting imprecise estimates can be disregarded [13]. (b) The shear dissipation of energy for sandwich cylindrical shells significantly surpasses the tensile energy dissipation, thus justifying the neglect of tensile deformations in the viscoelastic damping layer.

The sandwich cylindrical shell (see Figure 1) under investigation consists of three components: a base layer (cylindrical shell), a viscoelastic damping layer, and a constrained layer. The vibration of the base layer induces shear strain within the viscoelastic damping layer, which enables dissipation of energy and then effectively suppresses vibrations. The constrained layer is constructed from metal material and laid on the outer surface of the viscoelastic damping layer. The sandwich cylindrical shell contains a fluid referred to as *filling fluid*, while being surrounded by another fluid referred to as *surrounding free fluid*. The medium conditions are shown in Table 1.

In the cylindrical coordinate system, the analytical model is built as shown in Figure 1. Here, r, θ, and x represent radial, circumferential, and axial coordinates, respectively. The thickness and mean radius are denoted by h and R, respectively. The density, Young's modulus, shear modulus, and Poisson's ratio are denoted by ρ, E, G^*, and μ, respectively. The subscript i is added to these symbols to discriminate the base layer ($i = 1$), the viscoelastic damping layer ($i = 2$), and the constrained layer ($i = 3$). The shell is driven radially by a point force F located at (R_1, θ_0, x_0) in the cylindrical coordinate system (r, θ, x). The force is harmonic and has the time dependence of $\exp(-j\omega t)$, where ω is the angular frequency, t is the time, and j is the square root of -1. The relationship between geometric variables can be expressed as

$$R_2 = \frac{R_1 + (h_1 + h_2)}{2}, \qquad R_3 = \frac{R_1 + (h_1 + 2h_2 + h_3)}{2}. \tag{1}$$

The length of the model in Figure 1 is finite. Finite-shell vibrations exhibit the spatial periodicity distributed along the shell axis and have discrete axial wavenumber spectra. The finite-shell wavenumbers for different boundary conditions are shown in Table 2, where k_m is the axial wavenumber, m is the axial mode number (the number of half-wavelength along the shell axis, $m = 1, 2, 3 \ldots$), and L is the shell length.

2.2. Experimental Model. An experimental model, corresponding to the analytical one shown in Figure 1, is also constructed (see Figure 2). The geometric dimensions and material parameters are provided in Tables 3 and 4. The shell is sealed by end-caps which are supported by two rods passing through arranged holes on the end-cap. Each ring end-cap features a small hole (not depicted in Figure 2) for filling fluid into the shell. The boundary condition at the shell end can be considered as *simply supported*. In addition, a shaker is attached to the shell and provided as a harmonic point-force driver. The forced-vibration experiments for the experimental model are performed under three media conditions as shown in Table 1. The position of excitation is $(R_1, 0, L/6)$. Accelerometers are deployed at three measuring positions including position 1 $(R_3, \pi/2, 3L/4)$, position 2 $(R_3, \pi/4, L/2)$, and position 3 $(R_3, 0, L/3)$, respectively, as shown in Figure 2. The experimental platform is constructed as shown in Figure 3, which contains a sandwich cylindrical shell, shaker, sensors, and signal collector.

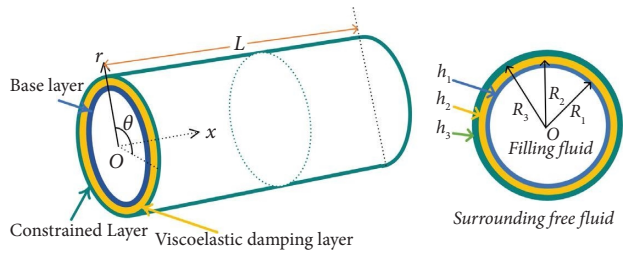

Figure 1: Analytical model.

Table 1: The medium conditions.

Case	Description	Inside shell	Outside shell
1	Fluid-filled	Water	Air
2	Fluid-loaded	Air	Water
3	Fluid-filled and -loaded	Water	Water

Table 2: Wavenumbers for different boundary conditions.

Boundary conditions	Wave numbers
Simply supported-simply supported (SS-SS)	$k_mL = m\pi$
Clamped-free (C-F)	$k_mL = (2m-1)\pi/2$
Clamped-clamped (C-C)	$k_mL = (2m+1)\pi/2$
Clamped-simply supported (C-SS)	$k_mL = (4m+1)\pi/4$

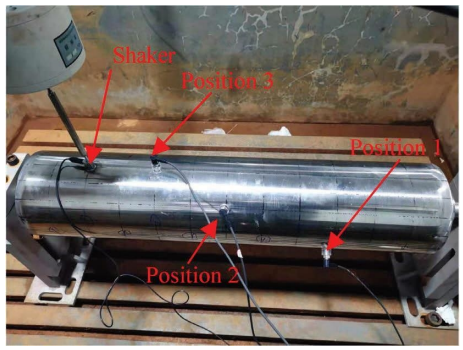

Figure 2: Experimental model.

Table 3: The geometric dimensions.

Symbol	L	R_1	h_1	h_2	h_3
Value	900	200	1.9	1.2	0.9

3. Vibroacoustic Modeling

3.1. Governing Equation of Motion. The governing equations for the motion of a sandwich cylindrical shell are derived in this section considering the force-displacement relationship. The force and moment acting on the base and constrained layers are described in detail as shown in Figures 4 and 5, respectively.

The axial and circumferential torsional displacements of the base layer and the constrained layer can be expressed as

$$\begin{cases} \beta_{xi} = -\dfrac{\partial w}{\partial x}, \\ \beta_{\theta i} = -\dfrac{1}{R_i}\dfrac{\partial w}{\partial \theta}, \end{cases} \tag{2}$$

where β_{xi} and $\beta_{\theta i}$ denote the axial and circumferential torsional displacements, respectively. The subscript i takes 1 for the base layer and 3 for the constrained layer.

The axial and circumferential torsional displacements of the viscoelastic damping layer can be expressed as

$$\begin{cases} \beta_{x2} = \dfrac{1}{h_2}\left(u_3 - u_1 - \dfrac{h_1}{2}\beta_{x1} - \dfrac{h_3}{2}\beta_{x3}\right), \\ \beta_{\theta 2} = \dfrac{1}{h_2}\left(v_3 - v_1 - \dfrac{h_1}{2}\beta_{\theta 1} - \dfrac{h_3}{2}\beta_{\theta 3}\right). \end{cases} \tag{3}$$

Shear strains of the viscoelastic damping layer can be expressed as

$$\begin{cases} \gamma_{xz} = \dfrac{\partial w}{\partial x} + \beta_{x2} = \dfrac{1}{h_2}(u_3 - u_1) + c_x\dfrac{\partial w}{\partial x}, \\ \gamma_{\theta z} = \dfrac{1}{R}\dfrac{\partial w}{\partial \theta} + \beta_{\theta 2} = \left(\dfrac{1}{h_2} - \dfrac{1}{2R_2}\right)v_3 - \left(\dfrac{1}{h_2} + \dfrac{1}{2R_2}\right)v_1 + c_\theta\dfrac{\partial w}{\partial \theta}, \end{cases} \tag{4}$$

where $c_\theta = h_3/2h_2R_3 + h_1/2h_2R_1 + h_1/4R_1R_2 - h_3/4R_2R_3 + 1/R_2$, $c_x = 1/2h_2(h_1 + 2h_2 + h_3)$.

Shear forces of the viscoelastic damping layer can be expressed as

$$\begin{cases} \tau_{xz} = G_2^*\gamma_{xz} = G_2^*\left(\dfrac{1}{h_2}(u_3 - u_1) + c_x\dfrac{\partial w}{\partial x}\right), \\ \tau_{\theta z} = G_2^*\gamma_{\theta z} = G_2^*\left(\left(\dfrac{1}{h_2} - \dfrac{1}{2R_2}\right)v_3 - \left(\dfrac{1}{h_2} + \dfrac{1}{2R_2}\right)v_1 + c_\theta\dfrac{\partial w}{\partial \theta}\right). \end{cases} \tag{5}$$

The balance of forces of the base layer or the constrained layer can be described as

$$\begin{cases} \dfrac{\partial N_{xi}}{\partial x} + \dfrac{1}{R_i}\dfrac{\partial N_{x\theta i}}{\partial \theta} + \tau_{xz} = \rho_i h_i\dfrac{\partial^2 u_i}{\partial t^2}, \\ \dfrac{1}{R_i}\dfrac{\partial N_{\theta i}}{\partial \theta} + \dfrac{\partial N_{\theta xi}}{\partial x} - \left(\dfrac{\partial M_{\theta i}}{R_i^2\partial \theta} + \dfrac{\partial M_{x\theta i}}{R_i\partial x}\right) + \tau_{\theta z} = \rho_i h_i\dfrac{\partial^2 v_i}{\partial t^2}, \\ \dfrac{\partial Q_{xi}}{\partial x} + \dfrac{1}{R_i}\dfrac{\partial Q_{\theta i}}{\partial \theta} + \dfrac{N_{\theta i}}{R_i} = \rho_i h_i\dfrac{\partial^2 w}{\partial t^2}. \end{cases} \tag{6}$$

The balance of moments of the base layer or the constrained layer can be described as

Table 4: The material constants.

Base layer			Stainless steel		
Density (kg/m^3)	ρ_1	7850	Young's modulus (GPa)	E_1	210
Poisson's ratio	μ_1	0.26	Loss factor	η_1	0.005
Viscoelastic damping layer			Rubber		
Density (kg/m^3)	ρ_2	1350	Loss factor	η_2	0.8
Shear modulus (MPa)	G_2^*	87	—	—	—
Constrained layer			Aluminum		
Density (kg/m^3)	ρ_3	2700	Loss factor	η_3	0.005
Young's modulus (GPa)	E_3	70	Poisson's ratio	μ_3	0.35
Fluid			Water		
Density (kg/m^3)	ρ_f	1000	Sound speed (m/s)	c_f	1500

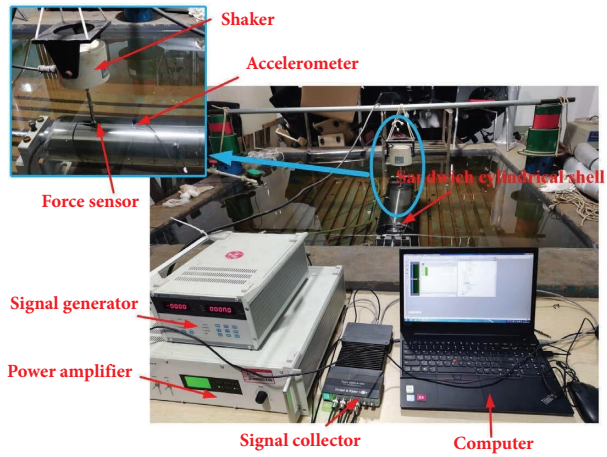

Figure 3: The experimental platform in the cistern.

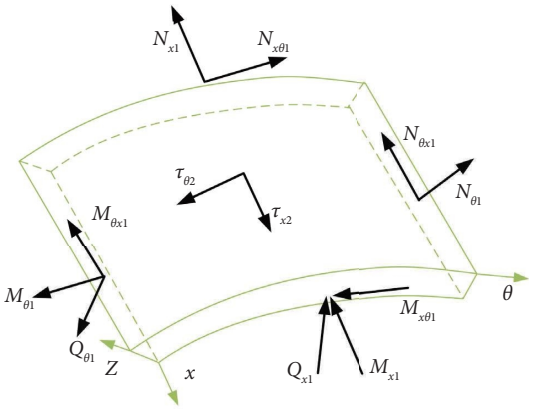

Figure 4: Unit force and moment acting on the base layer.

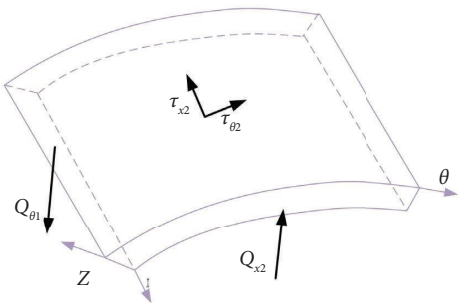

Figure 5: Unit force and moment acting on the constrained layer.

$$\begin{cases} \dfrac{1}{R_i}\dfrac{\partial M_{x\theta i}}{\partial y}+\dfrac{\partial M_{xi}}{\partial x}-Q_{xi}-\dfrac{h_i}{2}\tau_{xz}=0, \\ \dfrac{\partial M_{x\theta i}}{\partial x}+\dfrac{1}{R_i}\dfrac{\partial M_{\theta i}}{\partial \theta}-Q_{\theta i}-\dfrac{h_i}{2}\tau_{\theta z}=0. \end{cases} \tag{7}$$

By combining equations (6) and (7), we get

$$\begin{cases} \dfrac{\partial N_{xi}}{\partial x}+\dfrac{1}{R_i}\dfrac{\partial N_{x\theta i}}{\partial \theta}+\tau_{xz}=\rho_i h_i\dfrac{\partial^2 u_i}{\partial t^2}, \\ \dfrac{1}{R_i}\dfrac{\partial N_{\theta i}}{\partial \theta}+\dfrac{\partial N_{\theta xi}}{\partial x}-\left(\dfrac{\partial M_{\theta i}}{R_i^2\partial \theta}+\dfrac{\partial M_{x\theta i}}{R_i\partial x}\right)+\tau_{\theta z}=\rho_i h_i\dfrac{\partial^2 v_i}{\partial t^2}, \\ \dfrac{2\partial^2 M_{x\theta i}}{R_i\partial\theta\partial x}+\dfrac{\partial^2 M_{xi}}{\partial x^2}+\dfrac{h_i}{2}\dfrac{\partial \tau_{xz}}{\partial x}+\dfrac{1}{R_i^2}\dfrac{\partial^2 M_{\theta i}}{\partial \theta^2}+\dfrac{h_i}{2R_i}\dfrac{\partial \tau_{\theta z}}{\partial \theta} \\ \quad+\dfrac{N_{\theta i}}{R_i}=\rho_i h_i\dfrac{\partial^2 w}{\partial t^2}. \end{cases} \tag{8}$$

The stresses can be expressed as

$$\begin{cases} N_{xi}=K_i\left(\dfrac{\partial u_i}{\partial x}+\mu_1\dfrac{\partial v_i}{R_i\partial\theta}+\mu_i\dfrac{w}{R_i}\right), \\ N_{\theta i}=K_i\left(\mu_i\dfrac{\partial u_i}{\partial x}+\dfrac{w}{R_i}+\dfrac{\partial v_i}{R_i\partial\theta}\right), \\ N_{x\theta i}=K_i\dfrac{1-\mu_i}{2}\left(\dfrac{\partial v_i}{\partial x}+\mu_i\dfrac{\partial u_i}{\partial x}\right), \end{cases} \tag{9}$$

$$\begin{cases} M_{xi}=-D_i\left(\dfrac{\partial^2 w}{\partial x^2}+\mu_i\dfrac{\partial^2 w}{R_i^2\partial\theta^2}-\mu_i\dfrac{\partial v_i}{R_i^2\partial\theta}\right), \\ M_{\theta i}=-D_i\left(\mu_i\dfrac{\partial^2 w}{\partial\theta^2}-\dfrac{\partial v_i}{R_i^2\partial\theta}+\mu_i\dfrac{\partial^2 w}{\partial x^2}\right), \\ M_{x\theta i}=-D_i\dfrac{1-\mu_i}{2}\left(\dfrac{2\partial^2 w}{R_i\partial x\partial\theta}-\dfrac{\partial v_i}{R_i\partial\theta}\right), \end{cases} \tag{10}$$

where $K_i = E_i h_i/1-\mu_i^2$, $D_i = E_i h_i^3/12(1-\mu_i^2)$.

Only shear strain should be considered for the viscoelastic damping layer, the balance of which can be expressed as

$$\rho_2 h_2\frac{\partial^2 w}{\partial t}=-h_2\left(\frac{\partial \tau_{xz}}{\partial x}+\frac{\partial \tau_{\theta z}}{R_2\partial\theta}\right). \tag{11}$$

By combining equations (8)–(11), the governing equations of motion of the sandwich cylindrical shell can be finally obtained as

$$\begin{bmatrix} Q_{11} & Q_{12} & Q_{13} & Q_{14} & Q_{15} \\ Q_{21} & Q_{22} & Q_{23} & Q_{24} & Q_{25} \\ Q_{31} & Q_{32} & Q_{33} & Q_{34} & Q_{35} \\ Q_{41} & Q_{42} & Q_{43} & Q_{44} & Q_{45} \\ Q_{51} & Q_{52} & Q_{53} & Q_{54} & Q_{55} \end{bmatrix}\begin{bmatrix} u_1 \\ v_1 \\ u_3 \\ v_3 \\ w \end{bmatrix}=\begin{bmatrix} 0 \\ 0 \\ 0 \\ 0 \\ -q-f \end{bmatrix}, \tag{12}$$

where the elements of matrix $[Q]$ are differential operators with values, which are described in the appendix based on Flügge's thin-shell theory. q denotes the acoustic pressure, which is defined as the difference of the acoustic pressure between the surrounding free fluid field and the filling fluid field. f denotes the driving force. In addition, both q and f are defined as positive inward.

In light of the modal superposition theory and wave propagation approach, the displacements can be expressed as a superposition of symmetric and antisymmetric modes as follows:

$$\begin{cases} u_1(x,\theta,t)=\sum\limits_{\alpha,m,n} U_{1mn}\cos k_m x\sin\left(n\theta+\dfrac{\alpha\pi}{2}\right)e^{-j\omega t}, \\ v_1(x,\theta,t)=\sum\limits_{\alpha,m,n} V_{1mn}\sin k_m x\cos\left(n\theta+\dfrac{\alpha\pi}{2}\right)e^{-j\omega t}, \\ u_3(x,\theta,t)=\sum\limits_{\alpha,m,n} U_{3mn}\cos k_m x\sin\left(n\theta+\dfrac{\alpha\pi}{2}\right)e^{-j\omega t}, \\ v_3(x,\theta,t)=\sum\limits_{\alpha,m,n} V_{3mn}\sin k_m x\cos\left(n\theta+\dfrac{\alpha\pi}{2}\right)e^{-j\omega t}, \\ w(x,\theta,t)=\sum\limits_{\alpha,m,n} W_{mn}\sin k_m x\sin\left(n\theta+\dfrac{\alpha\pi}{2}\right)e^{-j\omega t}, \end{cases} \tag{13}$$

where $\alpha = 0, 1$; $m = 1, 2, 3\ldots$; and $n = 0, 1, 2\ldots$.

Substituting equation (13) into the left part of equation (12) yields

$$[Q][\Phi]=\sum_{\alpha,m,n}\operatorname{diag}\left(A_{mn}^{\alpha},B_{mn}^{\alpha},A_{mn}^{\alpha},B_{mn}^{\alpha},C_{mn}^{\alpha}\right)[S][\Psi], \tag{14}$$

where $[\Psi]=\left[U_{1mn}\ V_{1mn}\ U_{2mn}\ V_{2mn}\ W_{mn}\right]^{\mathrm{T}}$, $A_{mn}^{\alpha}=\sin(n\theta+\alpha\pi/2)\cos k_m x$, $B_{mn}^{\alpha}=\cos(n\theta+\alpha\pi/2)\sin k_m x$, $C_{mn}^{\alpha}=\sin(n\theta+\alpha\pi/2)\sin k_m x$.

The elements of matrix $[S]$ are described as follows:

$$
\begin{aligned}
&S_{11} = -K_1\left(k_m^2 + \frac{1-\mu_1}{2R_1^{\,2}}n^2\right) - \frac{G_2^*}{h_2} - \rho_1 h_1 \omega^2, S_{12} = K_1\frac{1+\mu_1}{2R_1}k_m n,\\
&S_{13} = \frac{G_2^*}{h_2}, S_{14} = 0, S_{15} = K_1\frac{\mu_1}{R_1}k_m + G_2^* c_x k_m;\\
&S_{21} = S_{12}, S_{22} = -K_1\left(\frac{n^2}{R_1^2} + \frac{1-\mu_1}{2}k_m^2\right) - G_2^*\left(\frac{1}{h_2} + \frac{1}{2R_2}\right) + \rho_1 h_1 \omega^2,\\
&S_{23} = 0, S_{24} = G_2^*\left(\frac{1}{h_2} - \frac{1}{2R_2}\right), S_{25} = -K_1\frac{n}{R_1^2} - G_2^* c_\theta n;\\
&S_{31} = S_{13}, S_{32} = 0, S_{33} = -K_3\left(k_m^2 + \frac{1-\mu_3}{2R_3^{\,2}}n^2\right) - \frac{G_2^*}{h_2} + \rho_3 h_3 \omega^2,\\
&S_{34} = K_3\frac{1+\mu_3}{2R_3}k_m n, S_{35} = K_3\frac{\mu_3}{R_3}k_m - G_2{}^* c_x k_m;\\
&S_{41} = 0, S_{42} = S_{24}, S_{43} = S_{34},\\
&S_{44} = -K_3\left(\frac{n^2}{R_3^{\,2}} + \frac{1-\mu_3}{2}k_m^2\right) - G_2{}^*\left(\frac{1}{h_2} + \frac{1}{2R_2}\right) - \rho_3 h_3 \omega^2,\\
&S_{45} = -K_3\frac{n}{R_3^{\,2}} - G_2{}^* c_\theta n;\\
&S_{51} = -S_{15}, S_{52} = K_1\frac{\mu_1}{R_1^2} + G_2^* c_\theta\left(1 + \frac{h_2}{2R_2}\right)n + D_1\frac{nk_m^2}{R_1^2} + D_1\frac{n^3}{R_1^4},\\
&S_{53} = S_{35}, S_{54} = K_3\frac{\mu_1}{R_3^2} + G_2^* c_\theta\left(1 + \frac{h_2}{2R_2}\right)n + D_3\frac{nk_m^2}{R_3^2} + D_3\frac{n^3}{R_3^4},\\
&S_{55} = \frac{K_1}{R_1^2} + \frac{K_3}{R_3^2} + G_2^* h_2\left(c_x^2 k_m^2 + c_\theta^2 n^2\right) + D_1\left(k_m^2 + \frac{n^2}{R_1^2}\right)^2 + D_3\left(k_m^2 + \frac{n^2}{R_3^2}\right)^2 - \left(\rho_1 h_1 + \rho_3 h_3\right)\omega^2.
\end{aligned}
\tag{15}
$$

3.2. Exciting Force. The driving force f in equation (12) can be expressed as

$$f = \frac{F}{R_1}\delta(x - x_0)\delta(\theta - \theta_0), \tag{16}$$

where F denotes the amplitudes of exciting force and δ is the Dirac delta function.

3.3. Acoustic Propagation in Fluid Field. The propagation of acoustic waves in a fluid field can be expressed by the following Helmholtz equation:

$$\frac{\partial^2 p_\kappa}{\partial r^2} + \frac{1}{r}\frac{\partial p_\kappa}{\partial r} + \frac{1}{r^2}\frac{\partial^2 p_\kappa}{\partial \theta^2} + \frac{\partial^2 p_\kappa}{\partial x^2} + k_0^2 p_\kappa = 0, \tag{17}$$

where $p_\kappa(r, \theta, x)$ expresses the acoustic pressure. Subscript κ takes 1 for the filling fluid and 2 for the surrounding free fluid. The wavenumber is $k_0 = \omega/c_f$, where c_f denotes sound speed.

According to the separation of variables method, the acoustic pressure $p_\kappa(r, \theta, x)$ in equation (17) can be expressed as

$$p_\kappa(r, \theta, x) = \sum_{\alpha,m,n} A_{\kappa mn} p_{\kappa m}(r) p_{\kappa m}(x) \sin\left(n\theta + \frac{\alpha\pi}{2}\right). \tag{18}$$

The Fourier integral transformation of equation (11) yields the following equation:

$$\widetilde{p}_\kappa(r, \theta, x) = \sum_{\alpha,m,n} A_{\kappa mn} p_{\kappa m}(r) \widetilde{p}_{\kappa m}(\lambda) \sin\left(n\theta + \frac{\alpha\pi}{2}\right), \tag{19}$$

where $\widetilde{p}_{\kappa m}(\lambda) =$. Substituting equation (19) into equation (17) yields the following n th-order Bessel's equation:

$$\frac{d^2 p_{\kappa m}(r)}{dr^2} + \frac{1}{r}\frac{dp_{\kappa m}(r)}{dr} + \left(k_r^2 - \frac{n^2}{r^2}\right) p_{\kappa m}(r) = 0, \tag{20}$$

where $k_r = \begin{cases} \sqrt{k_0^2 - \lambda^2} & (k_0 > \lambda) \\ \sqrt{\lambda^2 - k_0^2} & (k_0 < \lambda) \end{cases}$. Equation (20) yields the general solutions as follows:

$$p_{\kappa m}(r) = \begin{cases} a_\kappa J_n(k_r r) + b_\kappa Y_n(k_r r) & (k_0 > \lambda) \\ c_\kappa I_n(k_r r) + d_\kappa K_n(k_r r) & (k_0 < \lambda) \end{cases}. \tag{21}$$

3.4. Acoustic-Structure Coupling. According to the continuity of radial velocity at the fluid-shell interfaces, the boundary conditions can be expressed (ignoring the thickness of the shell) as

$$\dot{w}(r, \theta, x) = \frac{1}{j\omega\rho_f}\left(\frac{\partial p_\kappa}{\partial r}\right)_{r=R}, \tag{22}$$

where the dot denotes the time derivative and $R = \begin{cases} R_1 & (\kappa = 1) \\ R_3 & (\kappa = 2) \end{cases}$.

The fifth equation of equation (13) yields the following equation:

$$\dot{w}(r, \theta, x)|_{r=R} = \sum_{\alpha,m,n} \dot{W}_{mn} \sin\left(n\theta + \frac{\alpha\pi}{2}\right) f_m(x), \tag{23}$$

where $\dot{W}_{mn} = -j\omega W_{mn}$, $f_m(x) = \begin{cases} \sin k_m x \, (0 \le x \le L) \\ 0 \, (x < 0, x > L) \end{cases}$.

The Fourier integral transform of equation (23) yields the following equation:

$$\widetilde{\dot{w}}(r, \theta, \lambda)|_{r=R} = \sum_{\alpha,m,n} \dot{W}_{mn} \sin\left(n\theta + \frac{\alpha\pi}{2}\right) \widetilde{f}_m(\lambda), \tag{24}$$

where $\widetilde{f}_m(\lambda) = \int_{-\infty}^{+\infty} f_m(x) e^{-jx} dx$.

The definite solution of acoustic pressure can be obtained by combining the general solution equation (14) with boundary conditions equation (24). After the inverse Fourier integral transformation of the solutions, they can be expressed as

$$p_\kappa(r, \theta, x) = \frac{2\rho_f \omega^2 m}{L} \sum_{\alpha,m,n} \sin\left(n\theta + \frac{\alpha\pi}{2}\right) \int_0^{+\infty} \frac{G_\kappa(r) W_{mn}}{\sqrt{1 - \beta^2}} \frac{S_m(\beta)}{k_m^2 - k_0^2\beta^2} d\beta, \tag{25}$$

where $\beta = \lambda/k_0$, $\alpha = k_0\sqrt{1 - \beta^2}$.

$$S_m(\beta) = \begin{cases} -\sin\left(\dfrac{k_0 L}{2}\beta\right) \cdot \sin\left[k_0\beta\left(x - \dfrac{L}{2}\right)\right] (m = 2, 4, 6 \ldots) \\ \\ \cos\left(\dfrac{k_0 L}{2}\beta\right) \cdot \cos\left[k_0\beta\left(x - \dfrac{L}{2}\right)\right] (m = 1, 3, 5 \ldots) \end{cases}$$

$$G_1(r) = \begin{cases} \dfrac{J_n^{(2)}(k_r r)}{k_r^2 J_n^{'(2)}(k_r R)} (k_0 > \lambda) \\ \\ \dfrac{I_n(k_r r)}{k_r^2 I_n'(k_r R)} (k_0 < \lambda) \end{cases}, \tag{26}$$

$$G_2(r) = \begin{cases} \dfrac{H_n^{(2)}(k_r r)}{k_r^2 H_n^{'(2)}(k_r R)} (k_0 > \lambda) \\ \\ \dfrac{K_n(k_r r)}{k_r^2 K_n'(k_r R)} (k_0 < \lambda) \end{cases}.$$

Functions J_n and Y_n are the Bessel's functions of the first kind and second kind, respectively, I_n and K_n are the modified Bessel's functions, and H_n is the Hankel's function. The prime is added to these functions to denote differentiation with respect to r.

The radiation impedance of acoustic-structure coupling interaction can be defined as

$$ZI_{\kappa}(R) = 2\pi R\rho_f c_f \cdot \frac{4pm\pi}{\varepsilon_n k_0 L^2} \int_0^{+\infty} \frac{jG_{\kappa}(\alpha R)}{\sqrt{1-\beta^2}} \frac{N_{qm}(\beta)}{Q_{qm}(\beta)} d\beta, \tag{27}$$

where

$$Q_{qm}(\beta) = \left(k_0^2\beta^2 - k_m^2\right)\left[k_0^2\beta^2 - \left(\frac{q\pi}{L}\right)^2\right],$$

$$N_{qm}(\lambda) = \begin{cases} \sin^2\dfrac{k_0 L}{2}\lambda, & (q, m = 2, 4, 6\ldots), \\ \mp j \sin\dfrac{k_0 L}{2}\lambda \cos\dfrac{k_0 L}{2}\lambda, & (q \neq m), \\ \cos^2\dfrac{k_0 L}{2}\lambda, & (q, m = 1, 3, 5\ldots). \end{cases} \tag{28}$$

3.5. Solution and Description. Both sides of equation (12) are multiplied by diag $(A_{qp}^{\alpha}, B_{qp}^{\alpha}, A_{qp}^{\alpha}, B_{qp}^{\alpha}, C_{qp}^{\alpha})$ and then integrated along the inner and outer surfaces of the shell, respectively, where $p = 0, 1, 2, 3\ldots q = 1, 2, 3\ldots \alpha = 0, 1$. By using orthogonality, the equation of motion in Fourier integral form can be expressed as

$$\sum_{\alpha,m,n} [\Lambda][S][\Psi] = \left\{-\widehat{f} - \widehat{q}\right\}, \tag{29}$$

where

$$[\Lambda] = \begin{cases} \pi L\delta_{np}\delta_{mq}\mathrm{diag}\left(\dfrac{1}{\varepsilon_n}, \dfrac{1}{2}, \dfrac{1}{\varepsilon_n}, \dfrac{1}{2}, \dfrac{1}{\varepsilon_n}\right), & (\alpha = 1), \\ \pi L\delta_{np}\delta_{mq}\mathrm{diag}\left(\dfrac{1}{2}, \dfrac{1}{\varepsilon_n}, \dfrac{1}{2}, \dfrac{1}{\varepsilon_n}, \dfrac{1}{2}\right), & (\alpha = 0), \end{cases} \tag{30}$$

$$\widehat{f} = \sum_{\alpha,p,q} \frac{F}{R_1} \sin\left(p\theta_0 + \frac{\alpha\pi}{2}\right) \sin k_q x_0.$$

Due to the disparate fluid medium conditions on either side of the shell (see Table 1), the acoustic pressure can be categorized into the following three forms of expression:

(1) Case 1: $\widehat{q} = j\omega \sum_{m,n} ZI_1(R_1) W_{mn}$

(2) Case 2: $\widehat{q} = -j\omega \sum_{m,n} ZI_2(R_3) W_{mn}$

(3) Case 3: $\widehat{q} = -j\omega \sum_{m,n} [ZI_2(R_3) - ZI_1(R_1)] W_{mn}$

The radial displacements (W_{mn}) can be obtained by solving equation (32). Two parameters, related to the vibration of the shell, are defined as follows:

(1) The averaged quadratic velocity $\langle V_r^2 \rangle$ is as follows:

$$\left\langle V_r^2 \right\rangle = \frac{\omega^2}{2\varepsilon_n} \sum_{mn} W_{mn} W_{mn}^*, \tag{31}$$

where the asterisk indicates complex conjugation and ε_n is the Newman factor. The total of the averaged quadratic velocity is utilized to characterize the intensity of vibrations within a specific frequency range, denoted by $\langle V_r^2 \rangle_{\text{total}}$. In the following, both $\langle V_r^2 \rangle$ and $\langle V_r^2 \rangle_{\text{total}}$ are expressed in dB referenced to $2.5 \times 10^{-17}\mathrm{m}^2/s^2$.

(2) The acceleration $\langle A_r \rangle$ is calculated as

$$\langle A_r \rangle = -\omega^2 \sum_{mn} W_{mn}, \tag{32}$$

where $\langle A_r \rangle$ is expressed in dB referenced to $1 \times 10^{-6}\mathrm{m}/s^2$.

4. Calculation and Verification

Before calculating the radial displacement (W_{mn}) analytically, the dissipation of structural energy should be introduced into the abovementioned theory by treating Young's modulus as a complex quantity, namely, $E \longrightarrow E(1 - j\eta)$, and shear modulus as another complex quantity, namely, $G^* \longrightarrow G^*(1 - j\eta)$, where η denotes the loss factor. In addition, the number of modes used for structural displacement is the main factor affecting the accuracy of the solution. In the present case, a careful study of convergence was performed by increasing the number of modes, leading to the following choice: $m = 1, 2, \ldots, 10; n = 0, 1, \ldots, 9$. It should be pointed out that the values of the natural frequencies are determined from the peak locations of the forced response curves, instead of solving the eigenvalue problem.

4.1. Free Vibration of the Sandwich Cylindrical Shell in the Air. The validity of the analytical model is verified by comparing the real part of the complex eigenvalues $\omega^2 = \omega_0^2(1 + i\eta)$ obtained from the standard characteristic equation of the sandwich cylindrical shell with those obtained by the authors in reference [16]. The geometry and material constants of the considered shell are provided as follows: $h_1 = h_2 = h_3 = 1/3$ mm, $L = R = 100$ mm, $\mu_1 = \mu_3 = 0.3$, $E_1 = E_3 = 210$ GPa, $G_2 = (8.582 + 2.985i)$ MPa, $\rho_1 = \rho_3 = 7850\,\mathrm{kg/m^3}$, and $\rho_2 = 1340\,\mathrm{kg/m^3}$. The interior and exterior of the shell are air medium.

The results obtained from the present method and reference [16] are presented in Table 5. The vibration of the cylindrical shell is axisymmetrical for $n = 0$. It is observed that both sets of results demonstrate excellent agreement with each other.

Table 5: Comparison of the results for the sandwich cylindrical shell.

m	Reference [16]	Present method
1	2.44E9	2.44E9
2	2.47E9	2.47E9
3	2.50E9	2.50E9
4	2.56E9	2.56E9
5	2.66E9	2.66E9
6	2.85E9	2.85E9
7	3.15E9	3.15E9
8	3.59E9	3.60E9
9	4.23E9	4.24E9
10	5.11E9	5.12E9

4.2. Free Vibration of the Submerged Sandwich Cylindrical Shell. To validate the precision of the present model for vibration analysis of a submerged sandwich cylindrical shell, the natural frequencies are computed by the finite element software COMSOL. The geometric dimensions and material parameters are shown in Tables 3 and 4. The two ends of the sandwich cylindrical shell adopt simply supported boundaries. The comparison of natural frequencies of the sandwich cylindrical shell is calculated under three medium conditions as shown in Table 6. Obviously, the errors between them are extremely low. The analysis shows that the errors are mainly due to the differences between the nonlinear materials of the FEM and the linear materials of the analytical method. The dynamic properties of the damping materials used in the FEM are affected by the frequency.

5. Results and Discussion

The influences of boundary conditions, medium conditions, and parameters of the CLD on the vibration characteristics of the sandwich cylindrical shell are primarily investigated in this section. The geometric dimensions and material parameters are shown in Tables 3 and 4.

5.1. Influence of the Boundary Condition. The four commonly encountered boundary conditions are considered in the present study, as illustrated in Table 2. The spectrum of $\langle V_r^2 \rangle$ under different boundary conditions is depicted in Figure 6. The medium condition is Case 3. In order to conduct a more comprehensive analysis of the impact of boundary conditions on the vibrational characteristics of sandwich cylindrical shells, the corresponding $\langle V_r^2 \rangle_{\text{total}}$ within the whole frequency range is presented in Table 7, and the natural frequencies are illustrated in Figure 7.

The total of the averaged quadratic velocity, as shown in Table 7, is ranked in a descending order as C-F, C-SS, SS-SS, and C-C. However, overall, the boundary conditions have minimal impact on the total of the averaged quadratic velocity with a variation range of approximately 0.74 dB within frequencies below 1000 Hz.

It can be observed from Figure 7 that the natural frequency of the same mode follows a descending order from C-C, C-SS, and SS-SS to C-F when both the circumferential wave number and axial wave number are small. Conversely, higher-order modes are minimally affected by boundary conditions. The analysis reveals that the stiffness of the system is influenced by the boundary conditions, with maximum rigidity and natural frequency observed when both ends are fixed, which can be easily comprehended. In other words, the sequence of system stiffness under different boundary conditions is C-C, C-SS, SS-SS, and C-F, respectively, ultimately resulting in a variation in natural frequency.

5.2. Influence of the Medium Condition. The spectrum of $\langle V_r^2 \rangle$ under different medium conditions (see Table 1) is depicted in Figure 8, the corresponding $\langle V_r^2 \rangle_{\text{total}}$ within whole frequency range is presented in Table 8, and the natural frequencies are illustrated in Figure 9.

Figure 8 shows that under the influence of the fluid, the averaged quadratic velocity undergoes changes, leading to alterations in both the magnitude of the resonance peaks and natural frequencies. Notably, the spectrum curve of $\langle V_r^2 \rangle$ under Case 3 exhibits a significant leftward shift. In the frequency range of 0–450 Hz, the spectrum curve of $\langle V_r^2 \rangle$ under Case 1 and Case 2 aligns well. As the frequency increases, the spectrum curve of $\langle V_r^2 \rangle$ of Case 1 shifts leftwards with respect to that of Case 2, indicating a decrease in the resonance frequency. According to Figure 9, the natural frequencies of Case 2 at the low orders are basically the same as those of Case 1 except $n = 1$, while those of Case 2 at the high orders are slightly higher than those of Case 1. Table 8 shows that within the 1000 Hz range, $\langle V_r^2 \rangle_{\text{total}}$ follows an order from large to small: Case 3, Case 2, and Case 1. The variation of these two parameters is primarily ascribed to the influence exerted by the fluid. The additional mass of a heavy fluid (e.g., water) is generally considered to result in a reduction of natural frequency, whereas the additional damping leads to a decrease in the amplitude of vibrations.

5.3. Influence of the Constrained Layer Damping. In order to investigate the effects of the CLD on the vibration control of submerged sandwich cylindrical shells, the spectrum of $\langle V_r^2 \rangle$ with and without CLD under Case 3 is depicted in Figure 10, the $\langle V_r^2 \rangle_{\text{total}}$ of which is calculated to be 92.41 dB and 104.59 dB, respectively. The difference between the $\langle V_r^2 \rangle_{\text{total}}$ amounts to 12.18 dB. The results indicate that the influence of CLD on the vibration control of cylindrical shells is notably significant. Obviously, the damping effect is not ideal in the frequency bands of 0–150 Hz and 550–650 Hz, and except for these two frequency ranges the damping effect is extremely excellent, and almost all of the resonance peaks are significantly reduced.

5.4. Influence of Thickness of the Viscoelastic Damping Layer. In order to investigate the effects of the thickness of the viscoelastic damping layer on the vibration characteristics of submerged sandwich cylindrical shells, h_2 is defined as a ratio relative to h_1, and all other geometric parameters remained unchanged as indicated in Table 3. The medium condition involves fluid-filled and -loaded.

Table 6: Comparison of the natural frequencies for the sandwich cylindrical shell.

m	Case 1		Case 2		Case 3	
	Present method	FEM	Present method	FEM	Present method	FEM
1	150.2	151.2	336.1	334.1	243.7	241.7
2	461.5	460.3	782.7	781.1	558.3	555.6
3	776.1	774.5	1133.6	1132.2	783.8	781.8
4	1043.4	1040.1	1367.9	1363.7	954.3	952.4
5	1265.6	1261.2	1558.2	1555.0	1103.9	1101.9
6	1453.7	1450.1	1737.5	1734.3	1227.1	1223.1
7	1617.6	1613.6	1856.3	1854.3	1342.6	1340.4
8	1763.9	1761.2	1993.8	1993.1	1446.0	1444.6
9	1897.0	1892.5	2099.4	2095.2	1540.6	1540.0
10	2020.2	2017.2	2205.0	2201.0	1635.2	1632.1

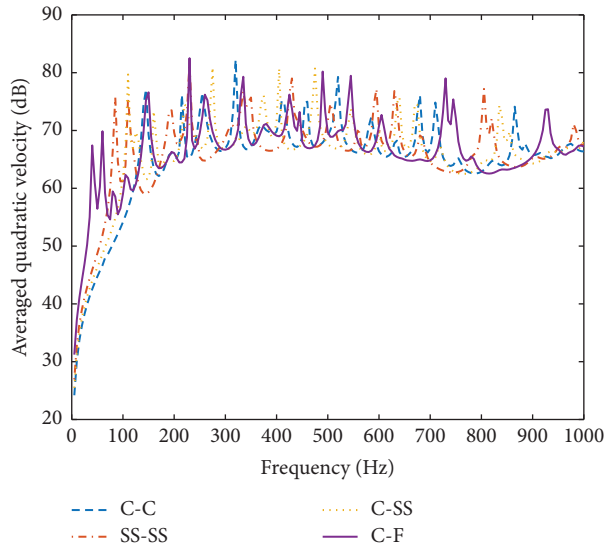

Figure 6: Averaged quadratic velocity under different boundary conditions.

Table 7: The total of the averaged quadratic velocity under different boundary conditions.

Boundary condition	C-C (dB)	SS-SS (dB)	C-SS (dB)	C-F (dB)
$\langle V_r^2 \rangle_{\text{total}}$	92.10	92.41	92.45	92.84

The spectrum of $\langle V_r^2 \rangle$ for different thicknesses of the viscoelastic damping layer is depicted in Figure 11, and the corresponding $\langle V_r^2 \rangle_{\text{total}}$ within the whole frequency range is presented in Table 9. It can be found that the averaged quadratic velocity decreases with the increase of thickness of the viscoelastic damping layer obviously on the whole, which can be primarily attributed to a thicker viscoelastic damping layer that facilitates greater dissipation. The results reveal the natural frequencies for different thicknesses of the viscoelastic damping layer, corresponding to various circumferential wave numbers and longitudinal half-wave numbers, which are depicted in Figures 12 and 13, respectively. Altering the thickness of the viscoelastic damping layer does not significantly affect the natural frequencies for lower circumferential modes and higher longitudinal modes. However, the natural frequency increases for both higher circumferential modes and lower longitudinal modes with the increasing thickness of the viscoelastic damping layer. The analysis reveals that the stiffness of a sandwich structure increases proportionally with the thickness of the viscoelastic damping layer, while the natural frequency decreases inversely with the stiffness. Moreover, the stiffness varies in different modes. Specifically, a larger number of circumferential modes or a smaller number of longitudinal modes results in more significant alterations in stiffness. Consequently, the natural frequency undergoes corresponding modifications.

To sum up, increasing the thickness of the viscoelastic damping layer enhances the damping properties of the composite structure in higher circumferential modes and lower longitudinal modes.

5.5. Influence of Thickness of the Constrained Layer. In order to investigate the effects of the thickness of the constrained layer on the vibration characteristics of submerged sandwich

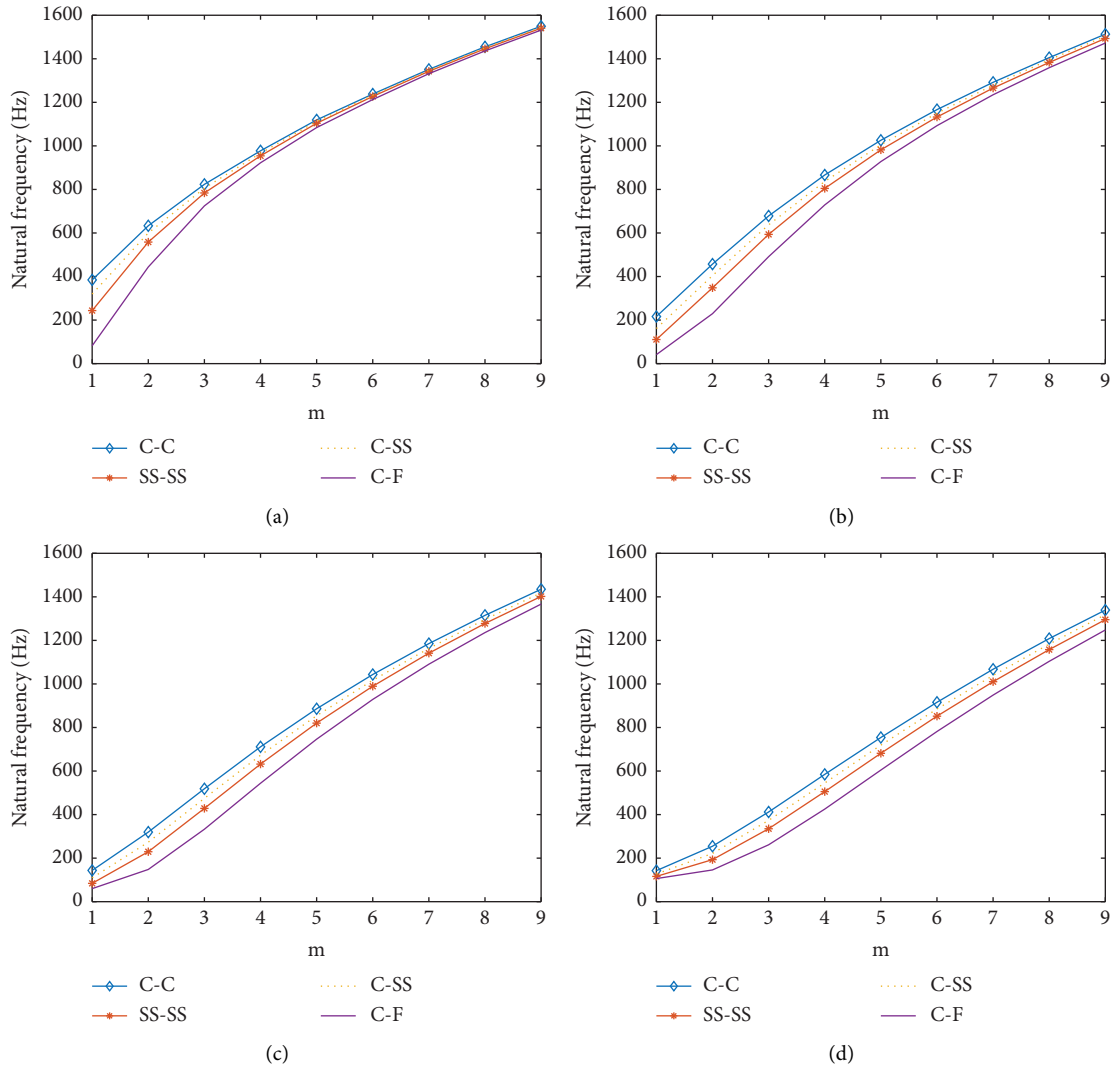

Figure 7: Natural frequency under different boundary conditions. (a) $n = 1$. (b) $n = 2$. (c) $n = 3$. (d) $n = 4$.

cylindrical shells, h_3 is defined as a ratio relative to h_1, and all other geometric parameters remained unchanged as indicated in Table 3. The medium condition involves fluid-filled and -loaded.

The spectrum of $\langle V_r^2 \rangle$ for different thicknesses of the constrained layer is depicted in Figure 14, and the corresponding $\langle V_r^2 \rangle_{\text{total}}$ within the whole frequency range is presented in Table 10. It can be found that the averaged quadratic velocity decreases with the increase of thickness of the constrained layer obviously. The analysis indicates that increasing the thickness of the constrained layer can introduce additional damping effects to the base, thereby exerting a vibration control influence. The natural frequencies for different thicknesses of the constrained layer, corresponding to various circumferential wave numbers and half-wave longitudinal wave numbers, are depicted in Figures 15 and 16, respectively. Increasing the thickness of the constrained layer enhances the damping properties of the composite structure. It can be observed that the natural frequency increases with the increasing thickness of the constrained layer, which is especially evident in higher modes. The analysis reveals that the stiffness of a sandwich structure increases proportionally with thickness of the constrained layer, while the natural frequency decreases inversely with the stiffness. Similarly, the stiffness varies in different modes. Specifically, a larger number of circumferential or longitudinal modes results in more significant alterations in stiffness.

6. Experiment and Analysis

6.1. Analytical and Experimental Results. The analytical and experimental results of the acceleration level at measuring position 3 are shown in Figures 17–19, respectively. The trends of the two spectral curves are essentially identical, with a satisfactory concurrence in the low-frequency range. Particularly, the resonance frequency in the low-frequency band is nearly identical.

By comparing the results, the analysis shows that the errors are mainly due to the following reasons:

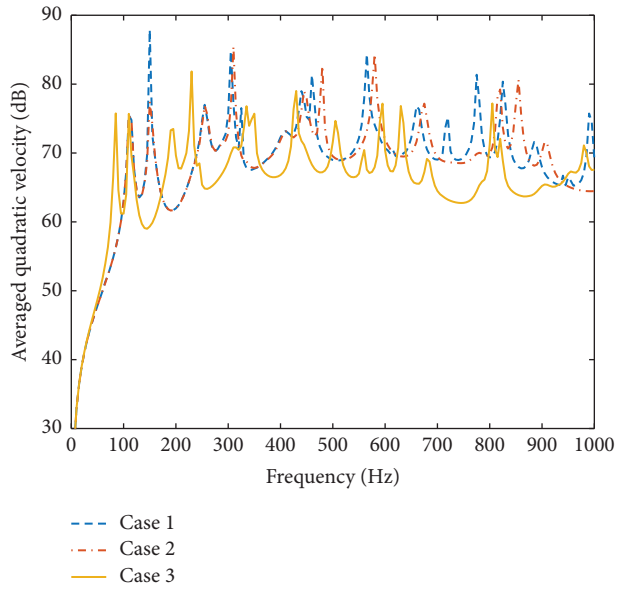

Figure 8: Averaged quadratic velocity under different medium conditions.

Table 8: The total of the averaged quadratic velocity under different medium conditions.

Case	1 (dB)	2 (dB)	3 (dB)
$\langle V_r^2 \rangle_{\text{total}}$	96.17	95.49	92.41

(1) The geometric parameters of the analytical and experimental models are difficult to be completely consistent. In contrast to the analytical model, the experimental model has an end-cap at each end, which results in a difference in natural frequencies.

(2) The boundary conditions of the analytical model are arduous to be identical to those of the experimental model. Experimentally, the simple-supported condition for the experimental model is not ideal, but the one for the analytical model is ideal in physical definitions.

(3) Under the current experimental conditions, it is almost impossible for the material parameters of the analytical and experimental models to be exactly the same. The shear modulus of rubber materials is characterized by frequency variability, while ideal materials are used in the analytical model, which leads to errors in the analytical results. As the frequency increases, the nonlinear changes in the damping properties of the elastic material become more and more pronounced, resulting in a tendency to make larger errors.

6.2. Experimental Analysis of the Vibration Control. To further analyze the effect of the CLD on the vibration control of the sandwich cylindrical shell, the experimental acceleration of the measuring position 3 with and without CLD is measured under three medium conditions.Figures 20–22 depict the acceleration of the position 3 to describe the effect of the CLD on the vibrational properties of the cylindrical shell under the three medium conditions. The following conclusions can be drawn from these figures:

(1) The constrained damping layer effectively controls the vibration of the cylindrical shell, and most of the resonant peaks are eliminated.

(2) The damping effect is not ideal within 150 Hz, but the damping effect is extremely excellent when it is larger than 200 Hz, and practically all formats are eliminated, which is consistent with the abovementioned theoretical analysis.

(3) The damping effects under Case 2 (fluid-loaded) and Case 3 (fluid-filled and -loaded) are similar and evidently stronger than that under Case 1 (fluid-filled). We can assume that the CLD has a noticeable damping effect in the whole frequency range.

From Table 11, we may state the following:

(1) The total vibration-level difference can reach above 5 dB in the frequency range of 1000 Hz under three medium conditions.

(2) The total vibration levels of the cylindrical shell without CLD are Case 1 (fluid-filled), Case 2 (fluid-loaded), and Case 3 (fluid-filled and -loaded) in order from large to small.

(3) The damping effects under Case 2 (fluid-loaded) and Case 3 (fluid-filled and -loaded) are similar and definitely stronger than that under Case 1 (fluid-filled).

To sum up, the analytical method presented in this paper is highly accurate and can directly reflect the physical relationship between excitation and response, which is of great significance for the optimization and design of various parameters of a sandwich cylindrical

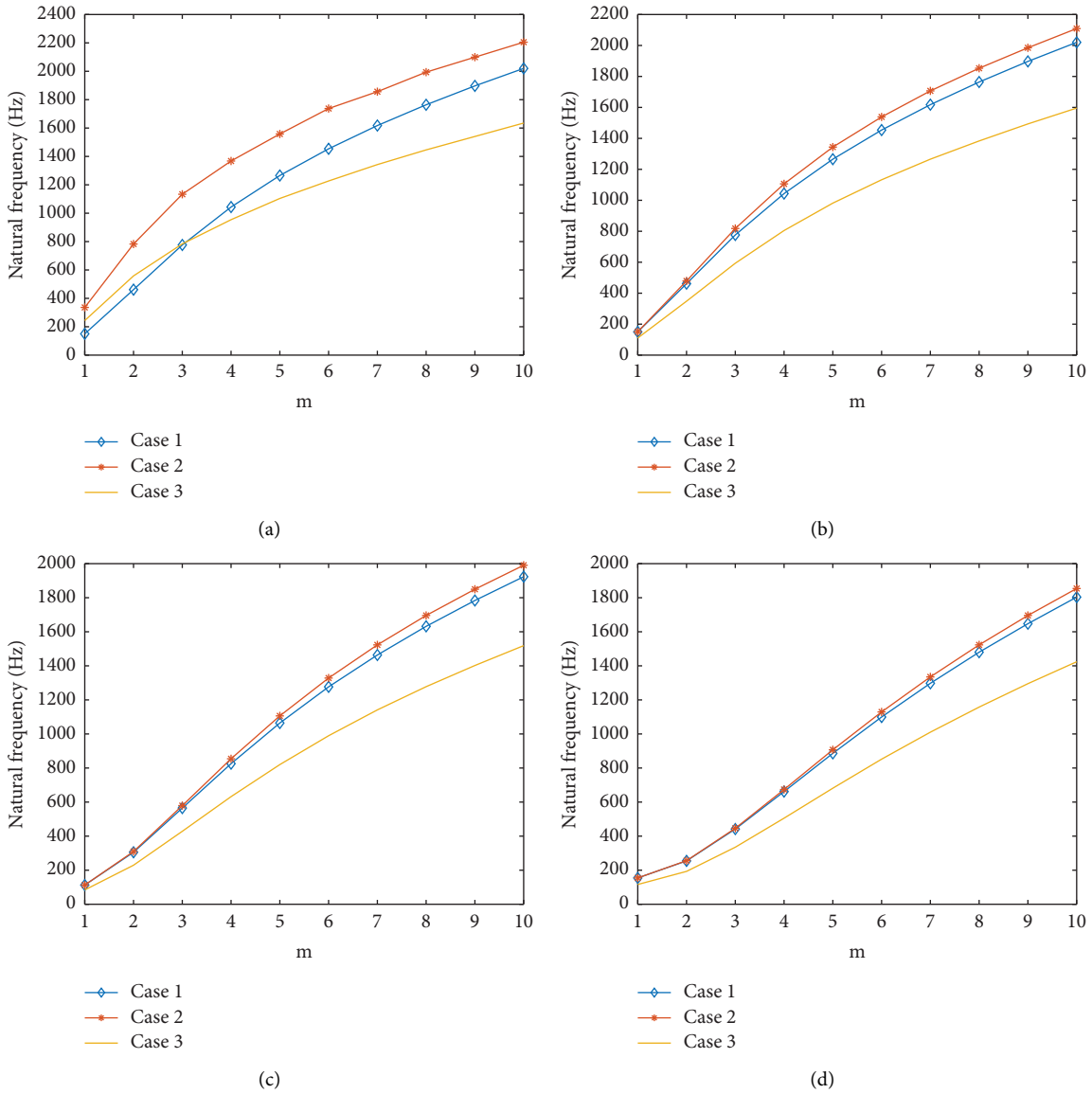

Figure 9: Natural frequency under different medium conditions. (a) $n = 1$. (b) $n = 2$. (c) $n = 3$. (d) $n = 4$.

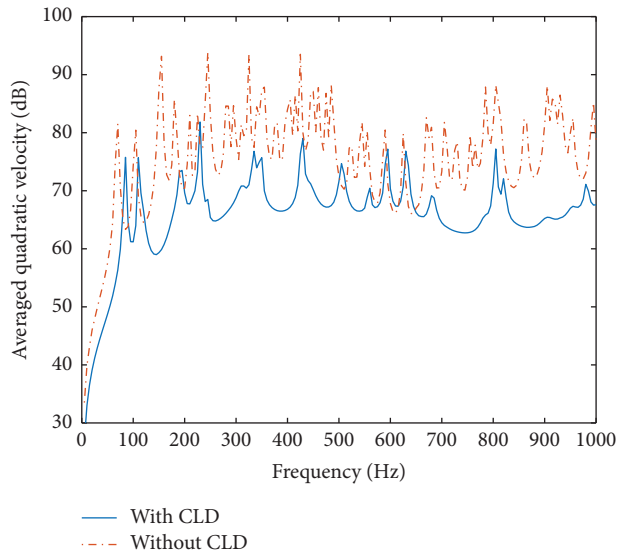

Figure 10: Averaged quadratic velocity with and without the constrained layer damping.

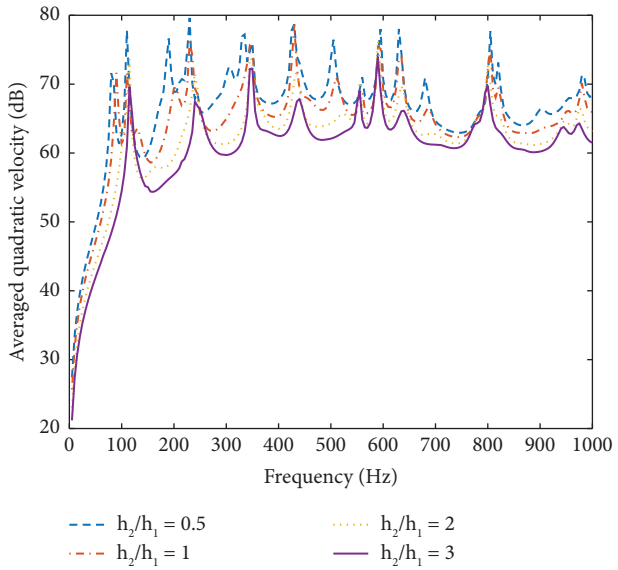

Figure 11: Averaged quadratic velocity for different h_2/h_1.

Table 9: The total of the averaged quadratic velocity for different h_2/h_1.

h_2/h_1	0.5 (dB)	1 (dB)	2 (dB)	3 (dB)
$\langle V_r^2 \rangle_{\text{total}}$	92.93	90.64	88.14	86.36

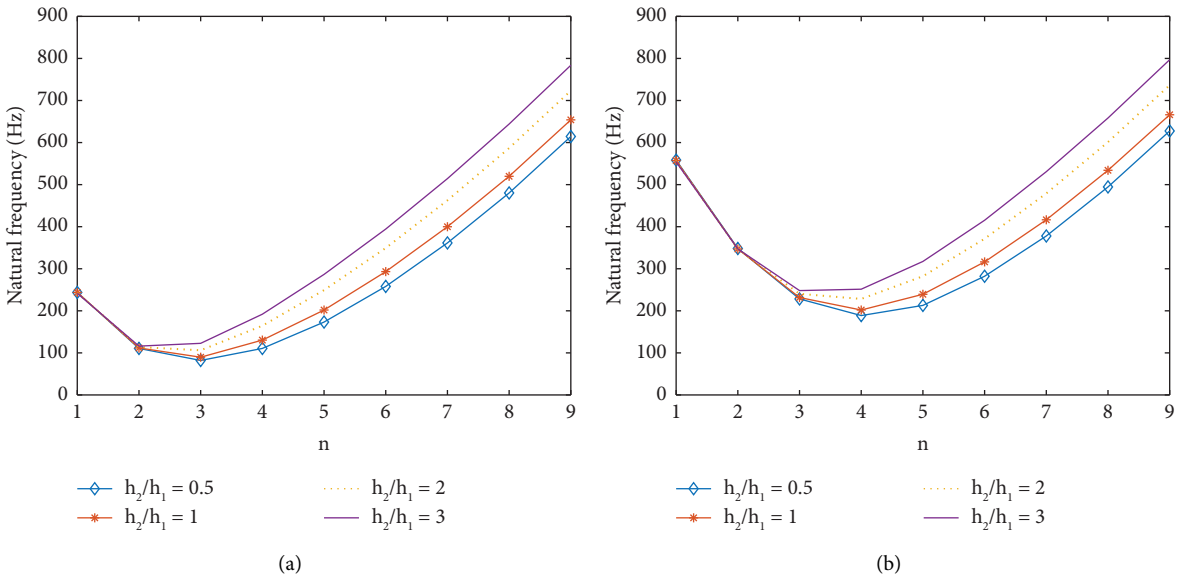

Figure 12: Natural frequency for different h_2/h_1. (a) $m = 1$. (b) $m = 2$.

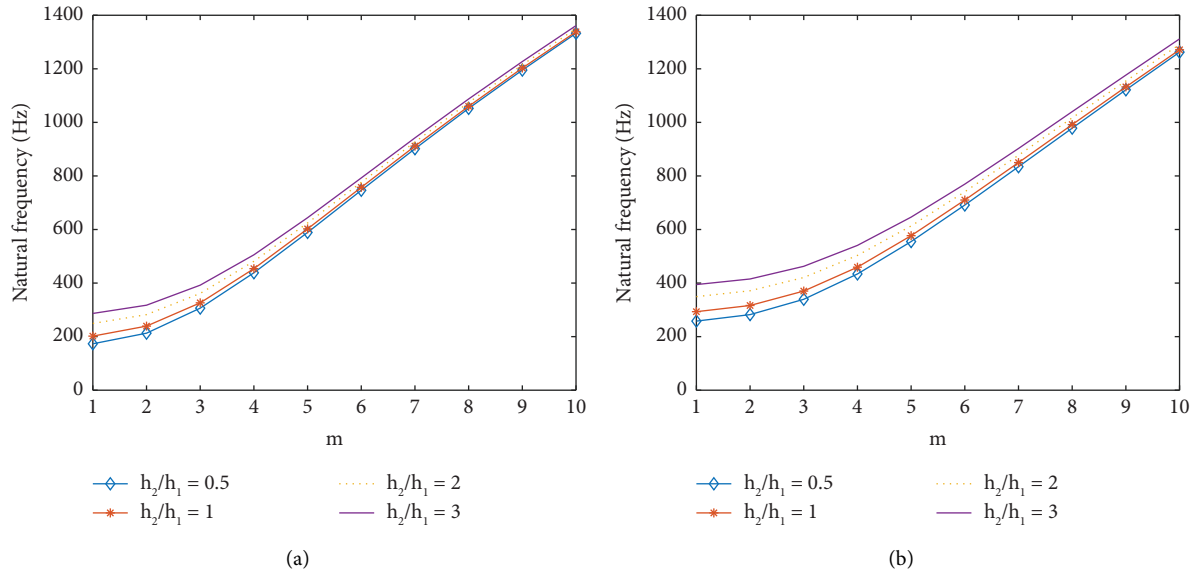

Figure 13: Natural frequency for different h_2/h_1. (a) $n = 5$. (b) $n = 6$.

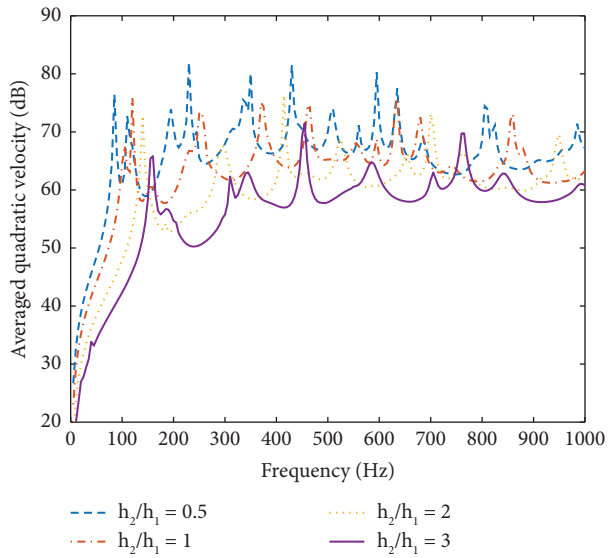

Figure 14: Averaged quadratic velocity for different h_3/h_1.

Table 10: The total of the averaged quadratic velocity for different h_3/h_1.

h_3/h_1	0.5 (dB)	1 (dB)	2 (dB)	3 (dB)
$\langle V_r^2 \rangle_{\text{total}}$	92.58	89.13	86.09	83.19

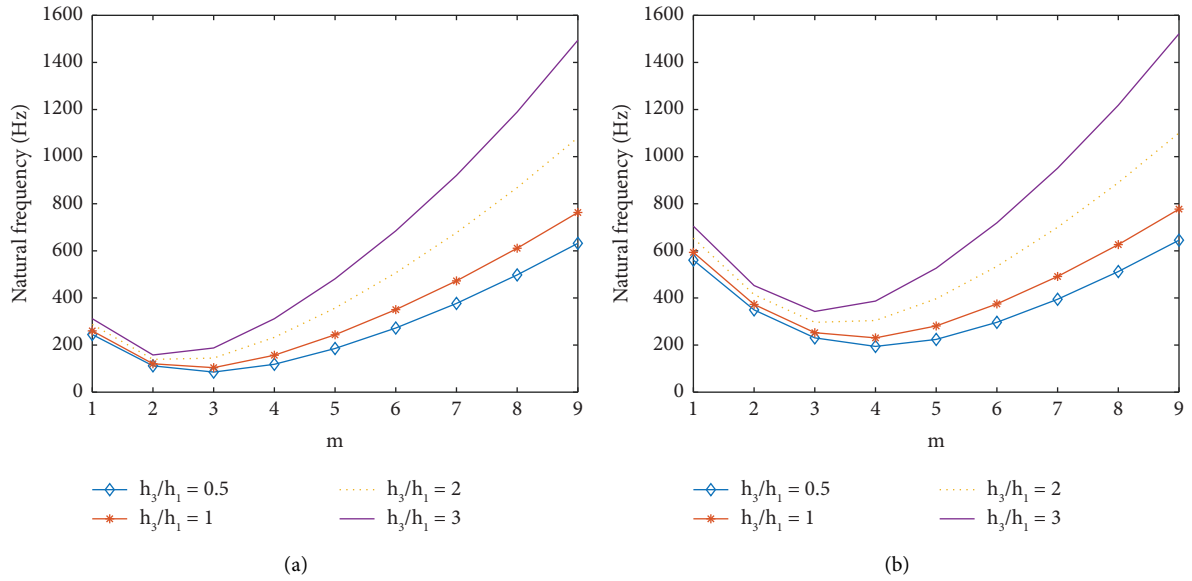

Figure 15: Natural frequency for different h_3/h_1. (a) $m = 1$. (b) $m = 2$.

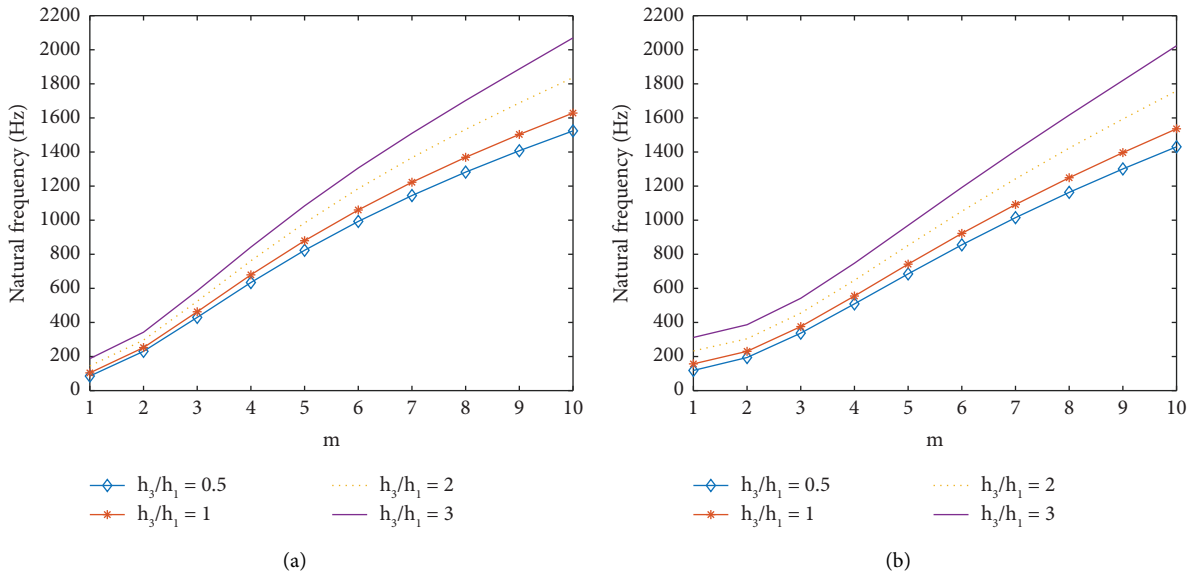

Figure 16: Natural frequency for different h_3/h_1. (a) $n = 3$. (b) $n = 4$.

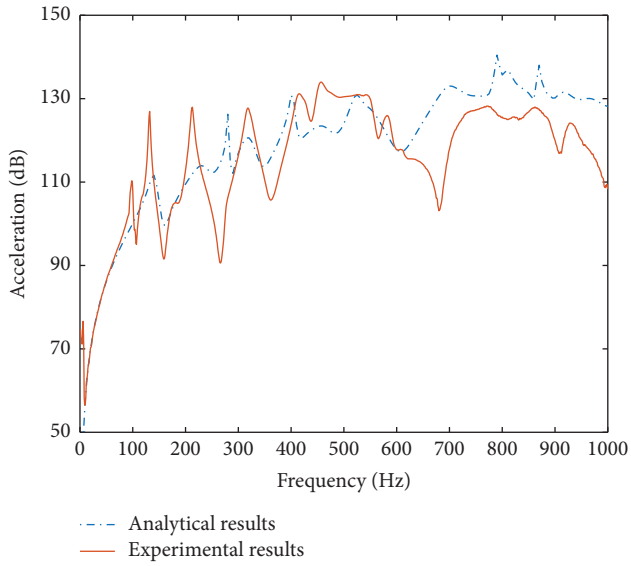

Figure 17: Acceleration under fluid-filled.

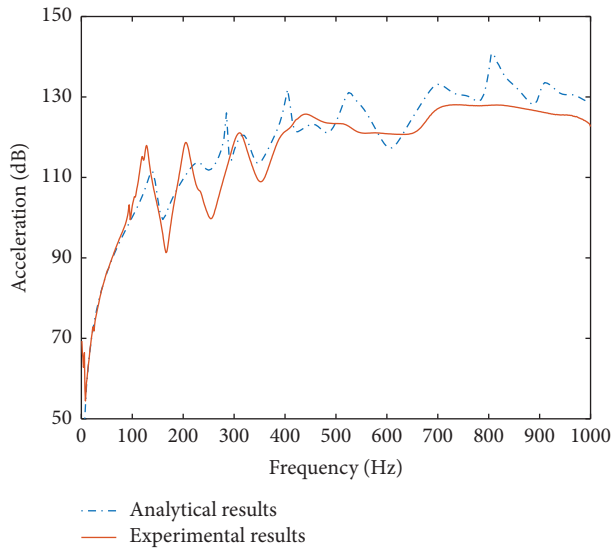

Figure 18: Acceleration under fluid-loaded.

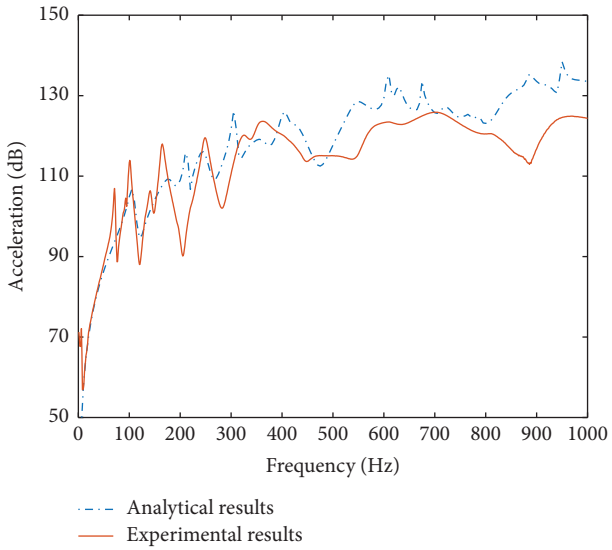

Figure 19: Acceleration under fluid-filled and -loaded.

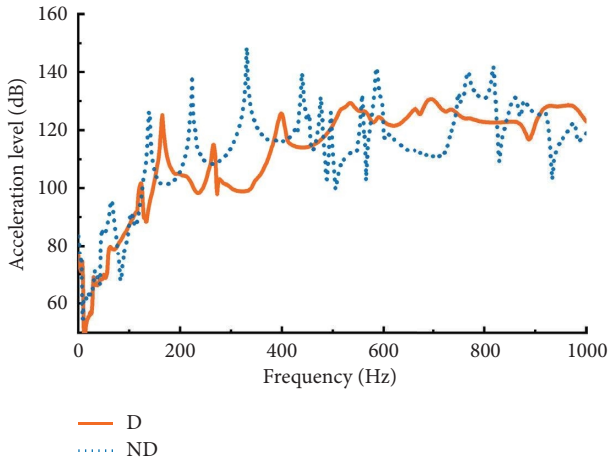

Figure 20: Damping effects under fluid-filled.

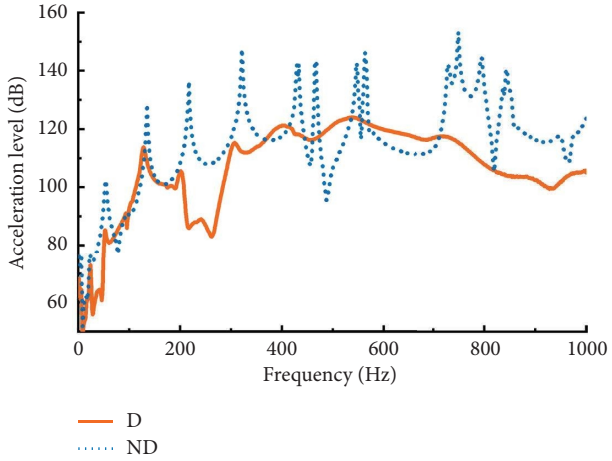

Figure 21: Damping effects under fluid-loaded.

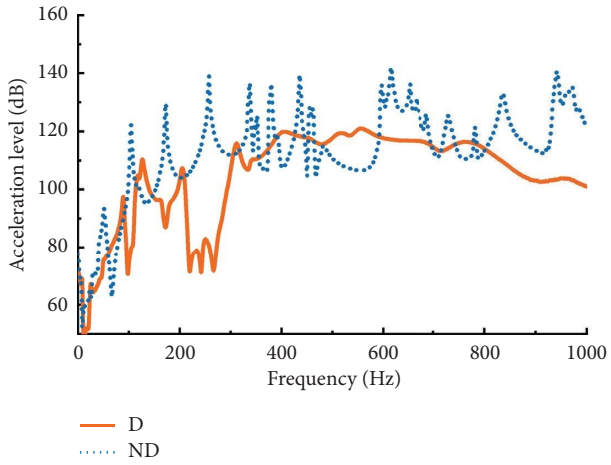

Figure 22: Damping effects under fluid-filled and -loaded.

Table 11: The total acceleration level obtained by the experiment under three medium conditions.

Case	Without CLD (dB)	With CLD (dB)	Difference (dB)
1	173.6	167.9	5.7
2	173.2	165.8	7.4
3	171.9	163.8	8.1

shell. Moreover, the CLD has a pronounced damping effect on a cylindrical shell under three medium conditions, which is a technically feasible approach in engineering.

7. Conclusion

An analytical model on the vibration of a point-driven sandwich cylindrical shell was proposed from the viewpoint of acoustic-structure coupling. The related experiments were performed. According to the reported results in this paper, the following conclusions can be drawn:

(1) On the basis of the relationship between force and displacement, an analytical model of sandwich cylindrical shells involving three medium conditions including fluid-filled, fluid-loaded, and fluid-filled and -loaded was proposed and verified.

(2) The rigidity of the system can be influenced by the boundary conditions. As the rigidity increases, so does the natural frequency. The stiffness of the system, under different boundary conditions (C-C, C-SS, SS-SS, and C-F), follows a descending order. Thus, this variation follows the same law in terms of natural frequency.

(3) The loading effect of the fluid medium mitigates the averaged quadratic velocity and natural frequencies of the cylindrical shell. The loading effect exhibits a gradient of intensity, ranging from fluid-filled and -loaded, fluid-loaded, to fluid-filled.

(4) Increasing the thickness of the viscoelastic damping layer enhances the damping properties of the composite structure in higher circumferential modes and lower longitudinal modes. Increasing the thickness of the constrained layer enhances the damping properties of the composite structure, which is especially evident in higher modes.

(5) Both theoretical and experimental results unequivocally demonstrate that the CLD has a pronounced damping effect on the cylindrical shell under three medium conditions, which is a technically feasible approach in engineering.

From the engineering point of view, the results presented in this paper are of strong reference for the study of vibration control in submerged sandwich cylindrical shells.

Appendix

Matrix [Q] in equation (12).

$$[Q] = \begin{bmatrix} Q_{11} & Q_{12} & Q_{13} & 0 & Q_{15} \\ Q_{12} & Q_{22} & 0 & Q_{24} & Q_{25} \\ Q_{13} & 0 & Q_{33} & Q_{34} & Q_{35} \\ 0 & Q_{24} & Q_{34} & Q_{44} & Q_{45} \\ Q_{15} & Q_{52} & Q_{35} & Q_{54} & Q_{55} \end{bmatrix}$$

$$\begin{aligned}
Q_{11} &= K_1\left(\frac{\partial^2}{\partial x^2} + \frac{1-\mu_1}{2{R_1}^2}\frac{\partial^2}{\partial \theta^2}\right) - \frac{G_2^*}{h_2} - \rho_1 h_1 \frac{\partial^2}{\partial t^2} \\
Q_{12} &= K_1 \frac{1+\mu_1}{2R_1}\frac{\partial^2}{\partial x \partial \theta} \\
Q_{13} &= \frac{G_2^*}{h_2} \\
Q_{15} &= K_1 \frac{\mu_1}{R_1}\frac{\partial}{\partial x} + G_2^* c_x \frac{\partial}{\partial x} \\
Q_{22} &= K_1\left(\frac{1}{R_1^2}\frac{\partial^2}{\partial \theta^2} + \frac{1-\mu_1}{2}\frac{\partial^2}{\partial x^2}\right) - G_2^*\left(\frac{1}{h_2} + \frac{1}{2R_2}\right) - \rho_1 h_1 \frac{\partial^2}{\partial t^2} \\
Q_{24} &= G_2^*\left(\frac{1}{h_2} - \frac{1}{2R_2}\right) \\
Q_{25} &= K_1 \frac{1}{R_1^2}\frac{\partial}{\partial \theta} + G_2^* c_\theta \frac{\partial}{\partial \theta} \\
Q_{33} &= K_3\left(\frac{\partial^2}{\partial x^2} + \frac{1-\mu_3}{2{R_3}^2}\frac{\partial^2}{\partial \theta^2}\right) - \frac{G_2^*}{h_2} - \rho_3 h_3 \frac{\partial^2}{\partial t^2} \\
Q_{34} &= K_3 \frac{1+\mu_3}{2R_3}\frac{\partial^2}{\partial x \partial \theta} \\
Q_{35} &= K_3 \frac{\mu_3}{R_3}\frac{\partial}{\partial x} - G_2^* c_x \frac{\partial}{\partial x} \\
Q_{44} &= K_3\left(\frac{1}{{R_3}^2}\frac{\partial^2}{\partial \theta^2} + \frac{1-\mu_3}{2}\frac{\partial^2}{\partial x^2}\right) - G_2^*\left(\frac{1}{h_2} + \frac{1}{2R_2}\right) - \rho_3 h_3 \frac{\partial^2}{\partial t^2} \\
Q_{45} &= K_3 \frac{1}{{R_3}^2}\frac{\partial}{\partial \theta} + G_2^* c_\theta \frac{\partial}{\partial \theta} \\
Q_{52} &= K_1 \frac{1}{R_1^2}\frac{\partial}{\partial \theta} + G_2^* c_\theta\left(1 + \frac{h_2}{2R_2}\right)\frac{\partial}{\partial \theta} \\
Q_{54} &= K_3 \frac{1}{R_3^2}\frac{\partial}{\partial \theta} - G_2^* c_\theta\left(1 - \frac{h_2}{2R_2}\right)\frac{\partial}{\partial \theta} \\
Q_{55} &= K_1 \frac{1}{R_1^2} + K_3 \frac{1}{R_3^2} - G_2^* h_2\left(c_x^2 \frac{\partial^2}{\partial x^2} + c_\theta^2 \frac{\partial^2}{\partial \theta^2}\right) + (D_1 + D_3)\nabla^2\nabla^2.
\end{aligned} \tag{A1}$$

Matrix $[Q]$ in equation (12).

$$\varepsilon_n = \begin{cases} 1 & (n = 0) \\ 2 & (n \neq 0) \end{cases} \quad \delta_{mq} = \begin{cases} 1, & (m = q), \\ 0, & (m \neq q), \end{cases} \quad \delta_{np} = \begin{cases} 1, & (n = p), \\ 0, & (n \neq p). \end{cases} \tag{A2}$$

Data Availability

The data used to support the findings of this study are available from the corresponding author upon reasonable request.

Conflicts of Interest

The authors declare that they have no conflicts of interest.

Acknowledgments

This study was supported by the Fund for the National Natural Science Foundation of China (nos. 52077218 and 51779098) and the Key Basic Research Projects of Basic Strengthening Program (no. 2020-JCJQ-ZD-222).

References

[1] H. Zheng, C. Cai, and X. M. Tan, "Optimization of partial constrained layer damping treatment for vibrational energy minimization of vibrating beams," *Computers and Structures*, vol. 82, no. 29-30, pp. 2493–2507, 2004.

[2] P. P. Hujare and A. D. Sahasrabudhe, "Experimental investigation of damping performance of viscoelastic material using constrained layer damping treatment," *Procedia Materials Science*, vol. 5, pp. 726–733, 2014.

[3] D. Zhang, Y. Wu, X. Lu, and L. Zheng, "Topology optimization of constrained layer damping plates with frequency- and temperature-dependent viscoelastic core via parametric level set method," *Mechanics of Advanced Materials and Structures*, vol. 29, no. 1, pp. 154–170, 2022.

[4] Z. Ling, X. Ronglu, W. Yi, and A. El-Sabbagh, "Topology optimization of constrained layer damping on plates using method of moving asymptote (mma) approach," *Shock and Vibration*, vol. 18, no. 1-2, pp. 221–244, 2011.

[5] G. Jin, C. Yang, Z. Liu, S. Gao, and C. Zhang, "A unified method for the vibration and damping analysis of constrained layer damping cylindrical shells with arbitrary boundary conditions," *Composite Structures*, vol. 130, no. oct, pp. 124–142, 2015.

[6] M. R. Permoon, H. Haddadpour, and M. Shakouri, "Nonlinear vibration analysis of fractional viscoelastic cylindrical shells," *Acta Mechanica*, vol. 231, no. 11, pp. 4683–4700, 2020.

[7] X. Cao, Z. Zhang, and H. Hua, "Free vibration of circular cylindrical shell with constrained layer damping," *Applied Mathematics and Mechanics*, vol. 32, no. 4, pp. 495–506, 2011.

[8] Y. Q. Guo, W. Q. Chen, and Y. H. Pao, "Dynamic analysis of space frames: the method of reverberation-ray matrix and the orthogonality of normal modes," *Journal of Sound and Vibration*, vol. 317, no. 3-5, pp. 716–738, 2008.

[9] T. C. Ramesh and N. Ganesan, "Finite element analysis of cylindrical shells with a constrained viscoelastic layer," *Journal of Sound and Vibration*, vol. 172, no. 3, pp. 359–370, 1994.

[10] H. J. Wang and L. W. Chen, "Finite element dynamic analysis of orthotropic cylindrical shells with a constrained damping layer," *Finite Elements in Analysis and Design*, vol. 40, no. 7, pp. 737–755, 2004.

[11] R. S. Masti and M. G. Sainsbury, "Vibration damping of cylindrical shells partially coated with a constrained viscoelastic treatment having a standoff layer," *Thin-Walled Structures*, vol. 43, no. 9, pp. 1355–1379, 2005.

[12] F. Abdoun, L. Azrar, and E. M. Daya, "Damping and forced vibration analyses of viscoelastic shells," *International Journal for Computational Methods in Engineering Science and Mechanics*, vol. 11, no. 2, pp. 109–122, 2010.

[13] F. Mohammadi and R. Sedaghati, "Linear and nonlinear vibration analysis of sandwich cylindrical shell with constrained viscoelastic core layer," *International Journal of Mechanical Sciences*, vol. 54, no. 1, pp. 156–171, 2012.

[14] L. H. Chen and S. C. Huang, "Vibration attenuation of a cylindrical shell with constrained layer damping strips treatment," *Computers and Structures*, vol. 79, no. 14, pp. 1355–1362, 2001.

[15] Y. C. Hu and S. C. Huang, "The frequency response and damping effect of three-layer thin shell with viscoelastic core," *Computers and Structures*, vol. 76, no. 5, pp. 577–591, 2000.

[16] Y. Xiang, Y. Y. Huang, J. Lu, L. Y. Yuan, and S. Z. Zou, "New matrix method for analyzing vibration and damping effect of sandwich circular cylindrical shell with viscoelastic core," *Applied Mathematics and Mechanics*, vol. 29, no. 12, pp. 1587–1600, 2008.

[17] L. Zheng, Q. Qiu, H. Wan, and D. Zhang, "Damping analysis of multilayer passive constrained layer damping on cylindrical shell using transfer function method," *Journal of Vibration and Acoustics*, vol. 136, no. 3, 2014.

[18] C. Yang, G. Jin, Z. Liu, X. Wang, and X. Miao, "Vibration and damping analysis of thick sandwich cylindrical shells with a viscoelastic core under arbitrary boundary conditions," *International Journal of Mechanical Sciences*, vol. 92, pp. 162–177, 2015.

[19] M. Mokhtari, M. R. Permoon, and H. Haddadpour, "Dynamic analysis of isotropic sandwich cylindrical shell with fractional viscoelastic core using Rayleigh–ritz method," *Composite Structures*, vol. 186, no. 2, pp. 165–174, 2018.

[20] P. Shahali, H. Haddadpour, and S. Shakhesi, "Dynamic analysis of electrorheological fluid sandwich cylindrical shells with functionally graded face sheets using a semi-analytical approach," *Composite Structures*, vol. 295, Article ID 115715, 2022.

[21] M. Permoon, M. Shakouri, and H. Haddadpour, "Free vibration analysis of sandwich conical shells with fractional viscoelastic core," *Composite Structures*, vol. 214, pp. 62–72, 2019.

[22] A. Askarian, M. Permoon, and M. Shakouri, "Vibration analysis of pipes conveying fluid resting on a fractional kelvin-voigt viscoelastic foundation with general boundary conditions," *International Journal of Mechanical Sciences*, vol. 179, Article ID 105702, 2020.

[23] M. V. Shitikova and B. Ajarmah, *Nonlinear Vibrations of Fractionally Damped Cylindrical Shells under the Additive Combinational Internal Resonance*, First International Nonlinear Dynamics Conference NODYCON 2019, Rome, Italy, 451–452, 2019.

[24] X. M. Zhang, "Frequency analysis of submerged cylindrical shells with the wave propagation approach," *International Journal of Mechanical Sciences*, vol. 44, no. 7, pp. 1259–1273, 2002.

[25] M. C. Junger and D. Feit, *Sound, Structures, and Their Interaction*, Cambridge, MA, USA, MIT press, 1986.
[26] K. Lam and C. Loy, "Effects of boundary conditions on frequencies of a multi-layered cylindrical shell," *Journal of Sound and Vibration*, vol. 188, no. 3, pp. 363–384, 1995.
[27] B. Laulagnet and J. L. Guyader, "Modal analysis of a shell's acoustic radiation in light and heavy fluids," *Journal of Sound and Vibration*, vol. 131, no. 3, pp. 397–415, 1989.
[28] C. R. Fuller and F. J. Fahy, "Characteristics of wave propagation and energy distributions in cylindrical elastic shells filled with fluid," *Journal of Sound and Vibration*, vol. 81, no. 4, pp. 501–518, 1982.
[29] C. R. Fuller, "The input mobility of an infinite circular cylindrical elastic shell filled with fluid," *Journal of Sound and Vibration*, vol. 87, no. 3, pp. 409–427, 1983.
[30] J. Scott, "The free modes of propagation of an infinite fluid-loaded thin cylindrical shell," *Journal of Sound and Vibration*, vol. 125, no. 2, pp. 241–280, 1988.
[31] X. Zhang, G. Liu, and K. Lam, "Coupled vibration analysis of fluid-filled cylindrical shells using the wave propagation approach," *Applied Acoustics*, vol. 62, no. 3, pp. 229–243, 2001.
[32] X. M. Zhang, "Parametric studies of coupled vibration of cylindrical pipes conveying fluid with the wave propagation approach," *Computers and Structures*, vol. 80, no. 3-4, pp. 287–295, 2002.
[33] Y. P. Guo, "Approximate solutions of the dispersion equation for fluid-loaded cylindrical shells," *Journal of the Acoustical Society of America*, vol. 95, no. 3, pp. 1435–1440, 1994.
[34] W. Williams, N. G. Parke, D. A. Moran, and C. H. Sherman, "Acoustic radiation from a finite cylinder," *Journal of the Acoustical Society of America*, vol. 36, no. 12, pp. 2316–2322, 1964.
[35] R. L. Bagley and J. Torvik, "Fractional calculus- a different approach to the analysis of viscoelastically damped structures," *AIAA Journal*, vol. 21, no. 5, pp. 741–748, 1983.
[36] G. Haneczok and M. Weller, "A fractional model of viscoelastic relaxation," *Materials Science and Engineering*, vol. 370, no. 1-2, pp. 209–212, 2004.
[37] F. C. Meral, T. J. Royston, and R. Magin, "Fractional calculus in viscoelasticity: an experimental study," *Communications in Nonlinear Science and Numerical Simulation*, vol. 15, no. 4, pp. 939–945, 2010.
[38] K. Adolfsson, M. Enelund, and P. Olsson, "On the fractional order model of viscoelasticity," *Mechanics of Time-Dependent Materials*, vol. 9, no. 1, pp. 15–34, 2005.
[39] L. E. Ramirez and C. F. Coimbra, "A variable order constitutive relation for viscoelasticity," *Annalen der Physik*, vol. 519, no. 7-8, pp. 543–552, 2007.
[40] Y. Qu, H. Hua, and G. Meng, "A domain decomposition approach for vibration analysis of isotropic and composite cylindrical shells with arbitrary boundaries," *Composite Structures*, vol. 95, pp. 307–321, 2013.
[41] G. Jin, T. Ye, Y. Chen, Z. Su, and Y. Yan, "An exact solution for the free vibration analysis of laminated composite cylindrical shells with general elastic boundary conditions," *Composite Structures*, vol. 106, pp. 114–127, 2013.
[42] A. Y. Guoqiang G and Z. Yinglong, "Analytical model of sandwich circular cylindrical shells underwater based on wave propagation approach," *Research Square (PREPRINT)*, 2023.